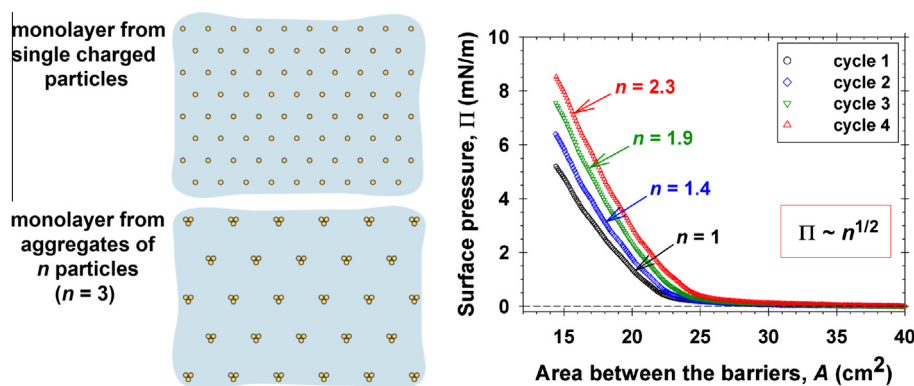# Monolayers of charged particles in a Langmuir trough: Could particle aggregation increase the surface pressure?

Plamen V. Petkov, Krassimir D. Danov, Peter A. Kralchevsky *

Department of Chemical & Pharmaceutical Engineering, Faculty of Chemistry & Pharmacy, Sofia University, 1164 Sofia, Bulgaria

GRAPHICAL ABSTRACT

ARTICLE INFO

ABSTRACT

The effect of aggregation on the surface pressure, Π, of monolayers from charged micrometer-sized colloidal particles on the air/water interface is investigated. Π is completely due to the long-range electrostatic repulsion between the particles mediated by their electrostatic field in the air. The most probable origin of particle aggregation is the attraction between capillary quadrupoles due to undulated contact lines on particle surfaces. Aggregates have higher charge and repel each other stronger than single particles. The data analysis by means of a theoretical model implies that Π linearly increases with $n^{1/2}$; n is the mean aggregation number, which can be determined from the experimental Π vs. area curves. The presence of electrolyte promotes aggregation, which tends to increase Π, but simultaneously reduces the surface charge that leads to lower Π. For our system, the first effect prevails and apparently paradoxical behavior is observed: the addition of salt in water enhances the electrostatic surface pressure. The data indicate limited aggregation: the rise of the electrostatic barrier prevents the further coalescence of aggregates if they have become sufficiently large. The results contribute for a better understanding of the factors that control the interactions in monolayers of charged particles at liquid interfaces.

© 2015 Elsevier Inc. All rights reserved.

1. Introduction

Non-densely packed monolayers from charged micron-sized particles on a liquid interface [1–3] have been investigated in view of their potential use for producing micro-patterned surfaces with applications for antireflective and superhydrophobic coatings [4–8], micro-lens arrays [9,10], structures in biosensing and bioengineering [11,12], and in relation to their importance for the interactions in Pickering emulsions [13–18], and for the phase-transfer catalysis [19,20]. The surface pressure isotherms for monolayers from charged particles have been studied

* Corresponding author.
E-mail address: pk@lcpe.uni-sofia.bg (P.A. Kralchevsky).

experimentally and theoretically for colloidal spheres at oil/water [3,21,22] and air/water [2,23] interfaces. Because the interparticle distances in such monolayers are of the order of several micrometers, i.e. much larger than the Debye length in the aqueous phase, the electrostatic interaction between the particles happens across the nonpolar fluid (air, oil). This interaction can be due to charges located at both the particle/water [24–29] and particle/nonpolar-fluid [3,13,15,30–38] interfaces. One possible origin of the electric charge at the particle/nonpolar-fluid interface can be the preferential adsorption of H^+ or OH^- ions from dissociated H_2O molecules in the atmospheric air [38–41] during the procedure of particle hydrophobization.

In experiments with optical tweezers, it was established that the effect of different hydrated counterions, Na^+, Rb^+ and Mg^{2+}, on the electrostatic repulsion between two particles at the oil/water interface is relatively weak [29,42]. Particle aggregation in monolayers of charged particles has been also observed and investigated [3,15,21,31]. Surface pressure isotherms with charged microgel particles at the oil/water interface have been measured, and it was concluded that the results are affected by the different shape and size of the microgel particles in their charged and uncharged states at the interface [43]. The effect of external uniform electrostatic field on uncharged [44] and charged [45] dielectric particles at a liquid interface was theoretically investigated.

From theoretical viewpoint, a particle of uniformly distributed surface charges, which is attached to a water/nonpolar-fluid interface, creates electric field that has a dipolar asymptotics. The force of electrostatic repulsion between two such particles (parallel dipoles) is [3,24–26]:

$$F_{ER} = \frac{3p_d^2}{2\varepsilon_n L^4} \quad (L \gg r_c, \kappa^{-1}), \tag{1}$$

where L is the center-to-center distance between the two particles; r_c is the radius of their contact lines; κ is the Debye screening parameter; ε_n is the dielectric constant of the nonpolar fluid

(air, oil); p_d is an effective dipole moment. The factor 2 in the denominator of Eq. (1) accounts for the fact that the dipolar field occupies only the upper half-space (the nonpolar fluid), whereas the electric field in the aqueous phase is screened by the ions in water.

If the charges are located at the *particle/nonpolar-fluid* interface (Fig. 1a), then the effective dipole moment p_d is [33]:

$$p_d = 4\pi\sigma \, D(\alpha_c, \varepsilon_{pn})R_p^3 \sin^3 \alpha_c \tag{2}$$

R_p is the particle radius, α_c is a central angle ($\sin\alpha_c = r_c/R_p$; for small deformations in the liquid interface created by the floating particle, we have $\alpha_c \approx \theta$, where θ is the contact angle); σ is the electric charge density at the particle/nonpolar-fluid interface; $D = D(\alpha_c, \varepsilon_{pn})$ is a known dimensionless function, which can be calculated by means of Table 1 and Eq. (D.1) in Ref. [33]; $\varepsilon_{pn} \equiv \varepsilon_p/\varepsilon_n$ is the ratio of the dielectric constants of the particle and nonpolar fluid.

If charges are located at the *particle/water* interface (Fig. 1b), then the effective dipole moment p_d can be estimated from the expression [25,26,28,29]:

$$p_d = \frac{4\pi\varepsilon_n\sigma_{pw}R_p^2(1 + \cos\alpha_c)}{\varepsilon_w\kappa}, \tag{3}$$

where ε_w is the dielectric constant of water; σ_{pw} is the electric charge density at the particle/water interface, and κ is the Debye screening parameter. Correspondingly, p_d given by Eq. (3) decreases upon the addition of electrolyte in the aqueous phase, whereas p_d expressed by Eq. (2) should be insensitive to the concentration of electrolyte in the water. Experimentally, this was observed with 1 μm sized silica particles at the octane/water interface – salt concentrations up to 1 M NaCl in the aqueous phase did not alter the interparticle distances [13]. In general, p_d might be a superposition of the contributions expressed by Eqs. (2) and (3). This superposition could be a sum or difference depending on whether the aforementioned two dipole moments have parallel or antiparallel orientation.
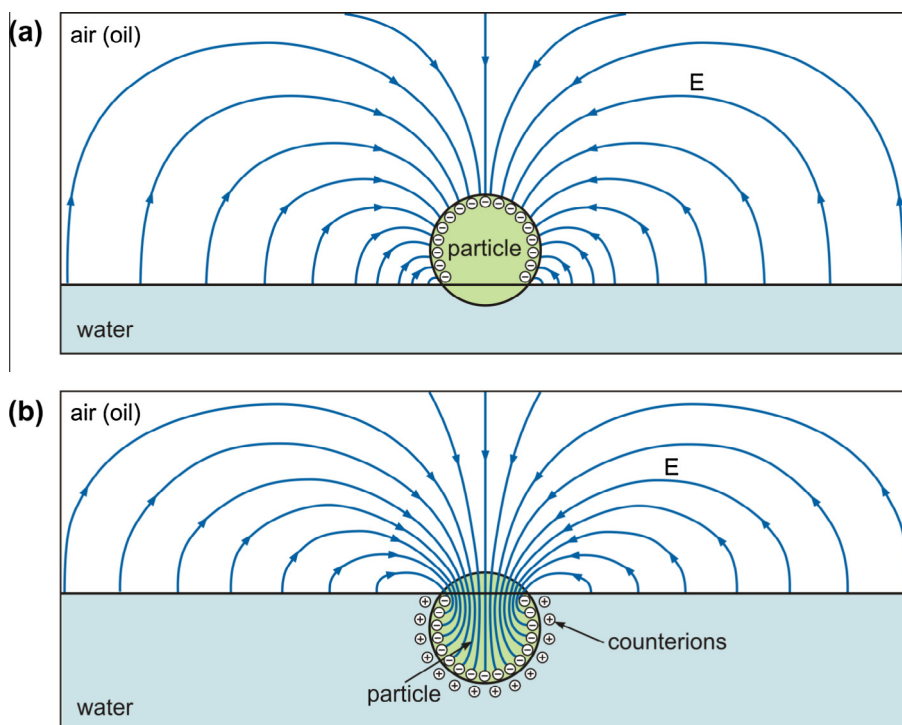

Fig. 1. Possible sources of the electric field in the nonpolar fluid (air, oil): (a) charges at the particle/nonpolar-fluid interface; (b) charges at the particle/water interface; their field can be weakened because of the effect of counterions in the aqueous phase.

In our previous study [23], it was experimentally established that the surface pressure of a monolayer of charged silica particles of radius $R_p \approx 2$ μm in a Langmuir trough asymptotically behaves as $\Pi \propto A^{-3/2}$ where A is the surface area (the area between the barriers in the trough). In other words, $\Pi \propto L^{-3}$, where L is the mean center-to-center distance between two particles in the monolayer. If the electrostatic interaction between two particles, described by Eq. (1), is assumed pair-wise additive then the summation over all pairs in the monolayer yields asymptotically $\Pi \propto L^{-5}$ [3]. The longer range of the experimental surface-pressure dependence ($\Pi \propto L^{-3}$) is due to collective effects, which have been taken into account in Ref. [23] by using the Bakker formula [46] with the Maxwell pressure tensor due to the electric field created by a periodic structure of charged particles at the liquid interface. The theoretical $\Pi(L)$ dependence obtained in this way is in agreement with the experimental data [23].

In subsequent experiments, we observed weak aggregation in monolayers of charged particles at the air/water interface. The aggregation was accompanied with enhancement of the surface pressure. Our goal in the present article is to investigate this effect. In other words, our goal is to clarify whether the aggregation of electrically charged particles could increase the surface pressure.

The structure of the paper is as follows. In Section 2, the materials and the experimental methods and procedures are described. In Section 3, zeta-potential data for the particles are reported and experimental $\Pi(A)$ isotherms with particles on the surface of pure water and aqueous KCl solutions are compared. In Section 4, theoretical interpretation of the obtained $\Pi(A)$ isotherms is proposed based on the model from Ref. [23]. Finally, in Section 5 we discuss the issues about the attractive force that causes the aggregation and about the origin of particle surface charges and the effect of electrolyte on the electrostatic surface pressure.

2. Materials, methods and procedures

2.1. Silica particles, hydrophobization and storage

The particles and the procedures for their hydrophobization and storage are the same as in our previous study [23]. For this reason, only a brief description is given here. The used silica particles Excelica UF305 were produced by Tokuyama Corp., Japan, by melting of synthetic SiO_2. The particles were spherical but polydisperse; see pictures of the particles obtained by scanning electron microscope (SEM) in Appendix A. During the cleaning procedure, the smallest Brownian particles were removed. The particles in the working suspension have a lognormal size distribution with maximum corresponding to radius $R_p = 1.92$ μm. The radii of 50% of the particles belong to the interval $1.56 \leqslant R_p \leqslant 2.37$ μm; see Ref. [23] for details.

Before an experiment, the particle surfaces were cleaned by means of the following procedure [23,37,47]. First, they were placed in sulfochromic acid for 2 h. Next, they were abundantly rinsed with water and then separated by centrifugation for 3 min at 5000 rpm. The rinsing was repeated three times. Further, the particles were placed in 0.01 M NaOH solution for 6 h. After that, they were rinsed with deionized water and left for 40 min to sediment. Finally, the particles were dried for 16 h at 80 °C.

The cleaned particles were hydrophobized with dichlorodimethylsilane (DCDMS, 99.5%, Fluka) following the procedure described in Ref. [23]. At the end of this procedure, the particles were dried for 40 min at 110 °C. If such dried particles are placed on the surface of water, they repel each other as visible from the considerable distances between them. By placing a needle-shaped electrode above the monolayer, we established that the particles are *negatively* charged; see Ref. [45] about the force acting on floating charged dielectric particles in external electric field. As already mentioned, a possible reason for surface charges on the particle/nonpolar-fluid interface could be the adsorption of ions from the atmospheric air [38–41]. It is known that the air contains 200–800 negative ions (mostly OH^-) per cm^3 at normal fair weather conditions [48].

The prepared charged particles were stored in a closed beaker with 20 mL isopropyl alcohol (IPA). Before each experiment, the glass beaker with the particle suspension in IPA was sonicated in water bath. After that, a portion of the suspension was taken with a pipette and spread on the surface of water in a Langmuir trough. The IPA evaporates and a particle monolayer is deposited on the water surface.

2.2. Experiments with particle monolayers in Langmuir trough

KSV NIMA Minimicro Langmuir trough was used. The particle monolayers formed in the trough were observed from below by an inverted microscope Axiovert 40 MAT (Carl Zeiss). The inner dimensions of the trough are $195 \times 51 \times 4$ mm. The surface pressure, Π, was measured using a Wilhelmy plate made of filter paper.

The trough was filled with the aqueous phase of volume 30 mL (thickness 3 mm). Several drops of the particle suspension in IPA were placed on the water surface between the barriers of the trough. If the particles have a greater charge (as seen from the larger interparticle distances) the amount of the spread suspension can be smaller. After that, we waited for 1–2 h until a stable constant value of Π is established. The surface area between the barriers varies from 85.6 to 14.4 cm^2 and vice versa in each cycle of monolayer compression (or expansion), which takes 840 s at a constant surface rate of 5.1 cm^2/min. Between the compression and expansion, we waited for 100 s to allow relaxation of the monolayer.

One of the compressions was carried out in a stepwise manner. At each step, different parts of the monolayer were recorded by video camera at a fixed distance between the barriers. From the video records, the average area per particle in the monolayer, α, was determined at different stages of compression. For this goal, images of the particle monolayer on video frames were subjected to numerical Delaunay triangulation and the respective Voronoi diagrams were constructed. Thus, the size distribution of the areas per particles was determined, and α was calculated as an arithmetic mean value; for details, see Ref. [23]. The plot of α vs. A is a straight line; see Fig. A2 in Appendix A. The slope is larger for particles of greater charge for which the area per particle, α, is greater. Because of the simple relation $A = N\alpha$, where N is the number of particles in the monolayer between the barriers, from the slope of the plot A vs. α one can determine N; see Appendix A.

Comparing the interparticle distances in the monolayer at a given degree of compression, we may conclude that the surface charge acquired by the particles in different hydrophobization runs is not perfectly reproducible, despite the fact that we are following exactly the same experimental procedure. Moreover, it was established [23] that the particle surface charge gradually decreases with the time of storage in IPA (the effect is noticeable for a period longer than one week). For these reasons, in a given series of experiments with the Langmuir trough we used particles from the same batch and the period of measurements was shorter than one week.

2.3. Zeta-potential measurements

The zeta-potential was measured with aqueous suspensions of the hydrophobized silica particles at various electrolyte concentrations. For this goal, the apparatus Zetasizer Nano ZS (Malvern Instruments, UK) was used. In these experiments, we used the fraction of smaller ($R = 0.8$–0.9 μm) silica particles of the original Excelica UF305 batch, which do not sediment. (We recall that in

the Langmuir-trough experiments the fraction of these smaller particles has been removed). In the zeta-potential measurements, the ionic strength has been $I > 10^{-5}$ M that corresponds to Debye length $\kappa^{-1} < 96$ nm, which is much smaller than the mean particle radius, i.e. the condition for correct measurement of zeta potential [49] is fulfilled.

The experimental procedure was the following. First, NaCl, KCl and NaI (products of Sigma–Aldrich) solutions of different concentrations (between 10^{-5} and 10^{-2} M) were prepared in small, 18 mL bottles. In each bottle, 2–3 drops of a freshly prepared suspension of hydrophobized silica particles in isopropyl alcohol were added. Next, the open bottles were kept for 2 h in a vacuum drier at room temperature to evaporate the isopropyl alcohol. The produced suspensions were stored for 18 h at 25 °C to achieve full equilibration between the particles and the electrolyte solution. Just before the zeta-potential measurement, the suspensions were sonicated in an ultrasonic bath to disperse the formed aggregates (if any).

The working temperature in all Langmuir-trough and zeta-potential measurements was 25 °C. All solutions were prepared with deionized water. Under the working conditions, dissolution of atmospheric CO_2 in the aqueous phase is possible, so that in the experiments with particle monolayers on the surface of water (without added salt) the aqueous phase may contain a background ionic strength of the order of 3.2×10^{-6} M.

3. Experimental results

3.1. Zeta-potential: results and discussion

The experimental procedure is described in Section 2.3. The experimental results shown in Fig. 2 are nontrivial. The negative zeta potential of the hydrophobized silica particles exhibits a minimum with the rise of electrolyte concentration for each of the three electrolytes, NaCl, KCl and NaI. To the left of the minimum, the values of the zeta potential are close for NaCl and KCl (with the same coion, Cl$^-$) but lower for NaI. To the right of the minimum, the magnitude of the zeta potential is smaller for the hydrophobized silica particles in the NaCl solution in comparison with the KCl solutions, the latter being close to the curve for NaI. The experimental curves in Fig. 2 can be interpreted as follows.

It is known that chloride and iodide anions [50,51], as well as other halide anions [52], exhibit specific binding to nonpolar surface patches of proteins. Hence, it is possible these anions to bind also to the hydrophobic patches on the surfaces of our hydrophobized silica particles. Such binding of Cl$^-$ and I$^-$ ions to the particle surfaces can explain the initial decrease of the zeta potential with the rise of electrolyte concentration.

The Na$^+$ and K$^+$ cations can also bind to the particle surface – most probably, for them the binding sites are the negative surface charges [53]. The shapes of the experimental curves in Fig. 2 indicate that the I$^-$ ions possess a higher binding energy, because their effect (increase of the magnitude of the negative surface potential) is stronger at the lower electrolyte concentrations. From this viewpoint, the coincidence of the experimental curves for NaCl and KCl can be explained with the fact that they have the same coion, Cl$^-$.

With the rise of electrolyte concentration, the negative surface potential is suppressed (i) due to the Debye screening effect and (ii) due to the binding of Na$^+$ and K$^+$ ions to the particle surfaces. At that, the Na$^+$ ions produce a greater effect (Fig. 2), which means that they have a higher binding energy than the K$^+$ ions for this specific hydrophobized-silica/water interface. Indeed, the minimum in the experimental curve appears at lower concentrations, and the values of the zeta potential are greater (less negative) for the curve with NaCl in comparison with that for KCl.
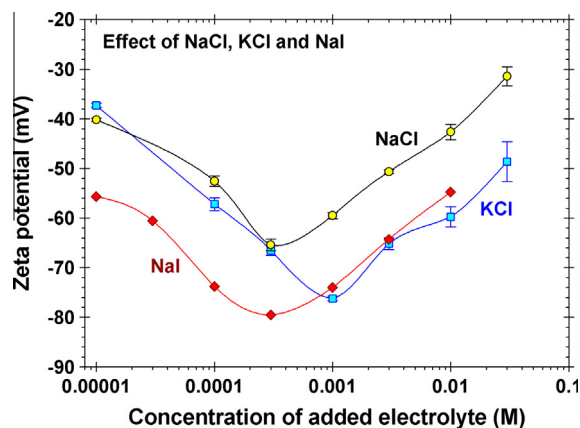
Fig. 2. Plots of data for the zeta potential of hydrophobized silica particles vs. the concentration of added electrolyte: NaCl, KCl and NaI; the lines are guides to the eye.

The most important result from these zeta-potential measurements is that the chloride and iodide anions can bind to the particle surfaces thus enhancing the negative surface potential of the silica particles. This result will be used below for discriminating between different possible hypotheses for explanation of the effect of electrolyte on the $\Pi(A)$ isotherms with monolayers of charged particles.

3.2. Particle monolayers on the surface of water

The experimental procedure is described in Section 2.2. Fig. 3a represents a SEM image of the used particles. One sees that the particles are spherical with smooth surfaces, but they are polydisperse. Fig. 3b is a photograph of the monolayer taken after cycle 1, which illustrates the appearance of surface aggregates after this compression/expansion cycle. The empty areas around the aggregates imply that the aggregates repel stronger their neighbors than the single particles.

Fig. 3c shows a series of surface-pressure isotherms, Π vs. A, corresponding to four consecutive compressions of the same monolayer of charged silica particles spread on the surface of water without any added electrolyte. (For brevity, this experiment will be further cited as "Experiment 1" with the Langmuir trough, where six drops of the particle suspension in IPA have been spread). Each compression is a part of a compression/expansion cycle; see Appendix A for more details. Fig. 3c shows a pronounced increase of Π with the number of cycle. The same data excellently comply with straight lines when plotted as Π vs. $A^{-3/2}$ (Fig. 3d) in accordance with the power dependence established in Ref. [23]:

$$\Pi = CA^{-3/2} + \Pi_0 \qquad (4)$$

Here, the coefficient C characterizes the slope of the experimental line and Π_0 is a background surface pressure. As seen in Fig. 3c, at the greatest expansions (lowest Π) the experimental $\Pi(A)$ dependences are very slant. This could be explained [23] with the fact that the electrostatic interaction has a certain range, so that above a given distance between the particles they are not strongly interacting and, thus, only a "gas" phase of particles is present. Our study is focused on the steep parts of the surface pressure isotherms. The slant part is taken into account by the additive constant Π_0 in Eq. (4).

Fig. 3d contains the experimental points from the steep portions of the curves in Fig. 3c. The values of the slope C and intercept Π_0 determined from the fits with linear regressions (Fig. 3d) are given in Table 1 (Experiment 1), where the regression coefficients are
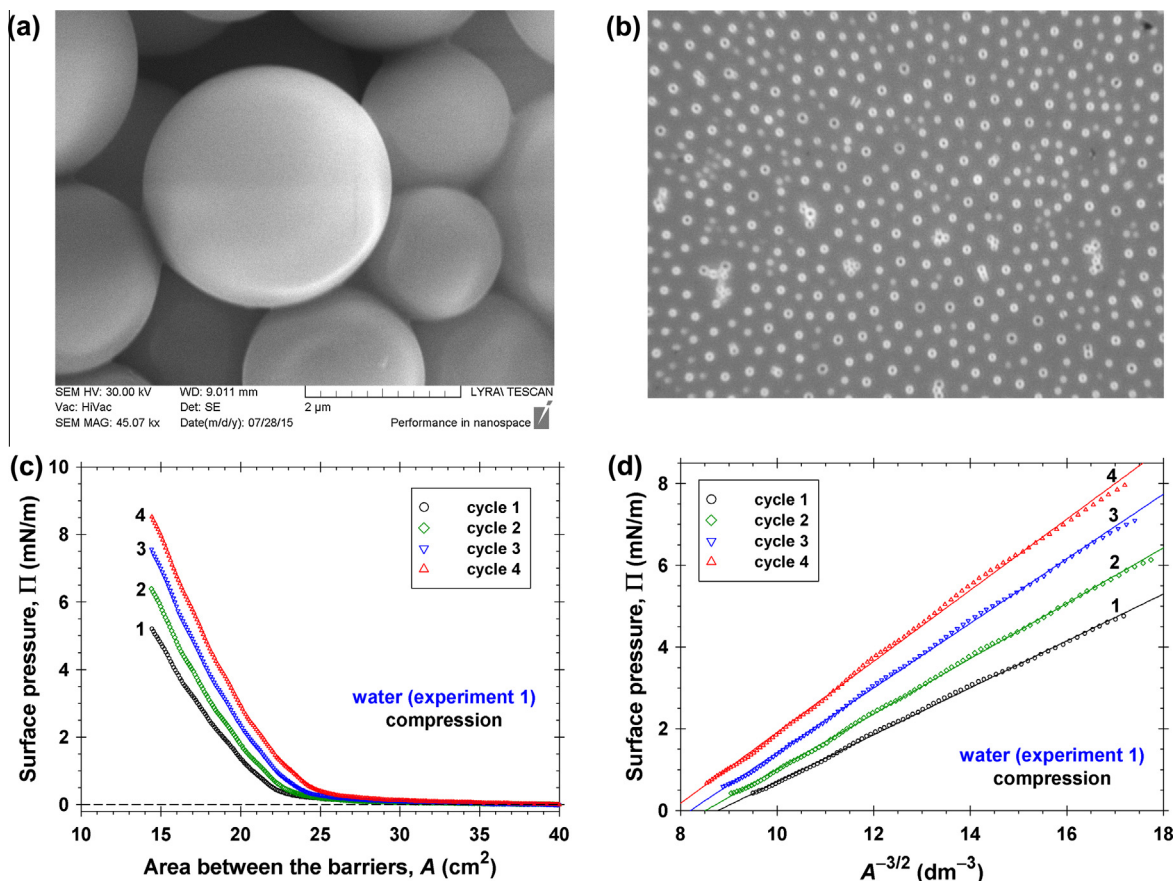
Fig. 3. (a) SEM micrograph of the used hydrophobized silica particles. (b) Monolayer of the same particles on the surface of water (the photographed domain is 289×217 μm). (c) Π vs. A isotherms measured in four consecutive cycles upon compression of the particle monolayer. (d) Data from the non-horizontal portion of the same $\Pi(A)$ isotherms, but this time plotted as Π vs. $A^{-3/2}$.

Table 1
Results from the fits of $\Pi(A)$ isotherms in accordance with Eq. (4).

Run	Slope C (mN cm^2)	Π_0 (mN/m)	Regr. coeff.
Experiment 1 (compression)			
Water, cycle 1	5.74 ± 0.02	−5.05 ± 0.02	0.9996
Water, cycle 2	6.77 ± 0.02	−5.77 ± 0.02	0.9997
Water, cycle 3	7.90 ± 0.02	−6.48 ± 0.03	0.9996
Water, cycle 4	8.69 ± 0.03	−6.78 ± 0.04	0.9994
Experiment 2 (compression)			
Water, cycle 1	4.15 ± 0.01	0.14 ± 0.02	0.9996
Water, cycle 2	4.16 ± 0.01	0.48 ± 0.02	0.9997
Water, cycle 3	4.37 ± 0.01	0.55 ± 0.02	0.9995
0.1 mM KCl[a]	7.88 ± 0.02	−5.59 ± 0.02	0.9997
1.0 mM KCl[a]	13.9 ± 0.04	−7.50 ± 0.04	0.9993

[a] The parameter values for KCl solutions are average over three cycles.

also given. It is seen that the slope C markedly increases with the number of the cycle. The behavior of the $\Pi(A)$ isotherms obtained upon expansion of the particle monolayer is similar; see Figs. A3–A7 in Appendix A. In Section 4.2, we verify the hypothesis that the particle aggregation could be a possible reason for the rise of Π after each cycle (as seen in Fig. 3c,d).

3.3. Effect of electrolyte on the $\Pi(A)$ isotherms

In this series of experiments, the same amount (8 droplets of the IPA suspension) of hydrophobized silica particles from the same batch was spread on the surface of aqueous phase containing 0, 0.1 and 1 mM KCl. (For brevity, this experiment will be further cited as "Experiment 2" with the Langmuir trough). In the "zero runs" without KCl, three compression/expansion cycles were carried out in the Langmuir trough. Qualitatively, the results are similar to those from Experiment 1. The values of C and Π_0 for Experiment 2 are also given in Table 1. The lower values of the slope C (Experiment 2, cycles 1–3 on the surface of water) indicate that in the case of Experiment 2 we are dealing with a batch of particles of lower charge as compared with Experiment 1 (see below).

In view of Fig. 2, where the magnitude of the negative zeta-potential of the particle/water interface increases in the concentration range 0.01–1 mM KCl, we expected to detect increase of the interparticle repulsion with the rise of the KCl concentration. In contrast, as seen in Fig. 4, we observed an increasing aggregation with the rise of electrolyte concentration. The results of this series of experiments are described in details in Appendix A; see Figs. A8 and A9 therein. Here, we present only the most interesting and important results.

Other surprising fact was the observed increase of Π with the rise of KCl concentration (Fig. 5a), despite the increasing aggregation (Fig. 4). As seen in Fig. 5a, for $A < 26$ cm^2 the experimental Π for 1 mM KCl becomes considerably greater than without added electrolyte in the water phase. The three isotherms in Fig. 5 exhibit broad linear portions when plotted as Π vs. A in accordance with Eq. (4); see Fig. 5b, where the slope of the lines increases with the rise of KCl concentration.

The particle contact angle at the air/water interface, θ, was measured by side-view observations like those in Ref. [3]. The average value from many photos of particles is $\theta = 94° \pm 2°$; see the inset in Fig. 5a. Detectable effect of the presence of KCl in the aqueous phase on the value of θ was not observed, in agreement with the results of other authors [21,29,42].
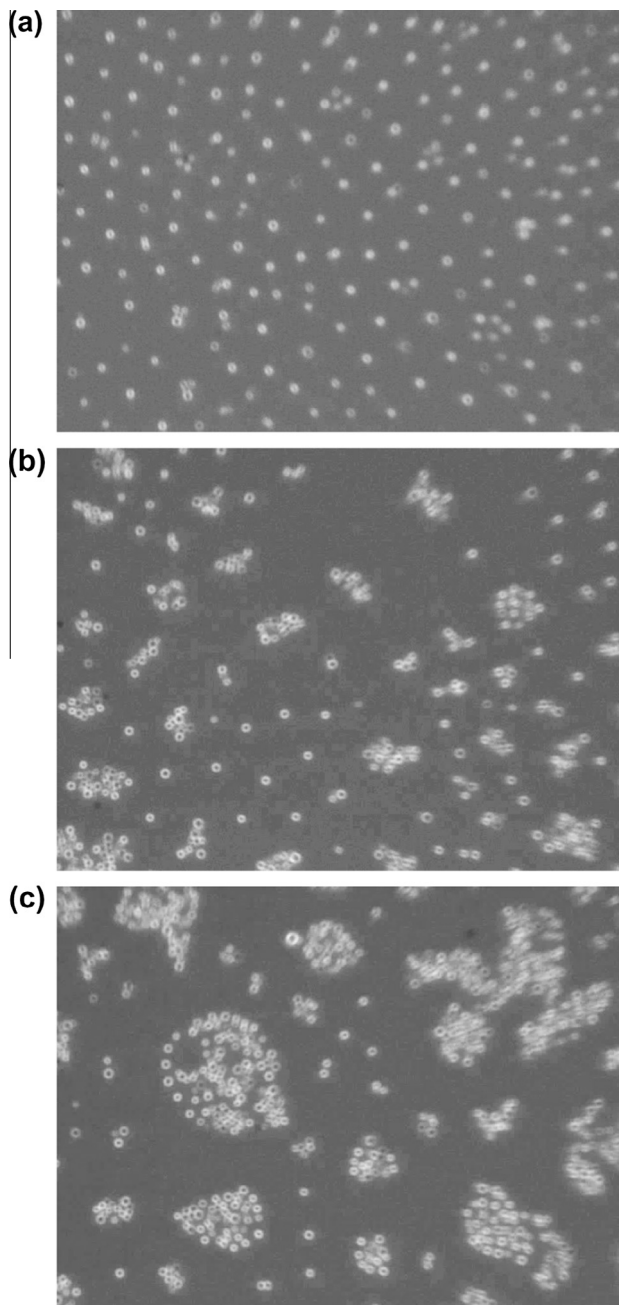
Fig. 4. Photographs of monolayers from hydrophobized silica particles on the surface of aqueous solution that contains (a) 0 mM; (b) 0.1 mM, and (c) 1 mM KCl (experiment #2); the photos show domains of size 289 × 217 μm.
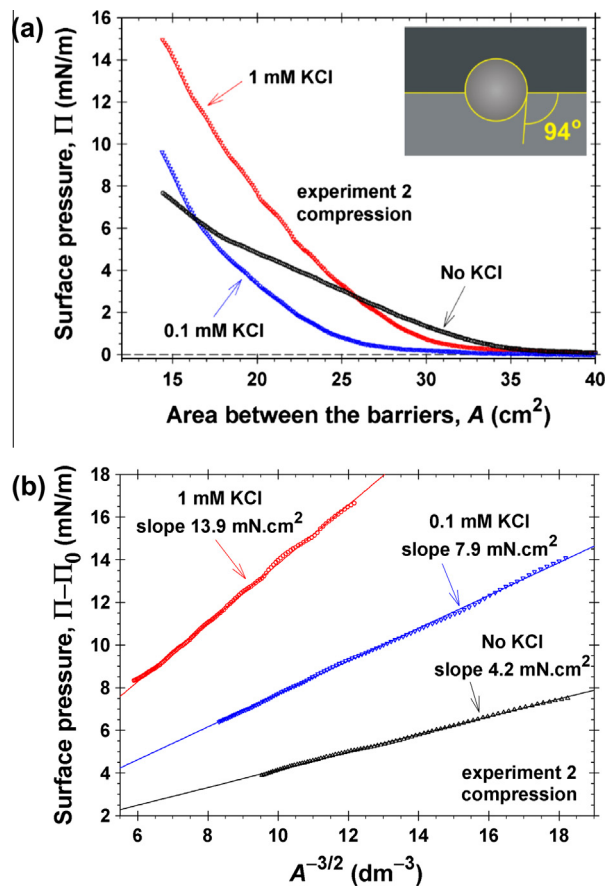

Fig. 5. (a) Plots of Π vs. A for monolayers containing the same amount of silica particles spread on the surface of an aqueous solution of 0, 0.1 and 1 mM KCl; experiment #2, cycle 1, compression; the inset illustrates the contact angle of the used particles. (b) The electrostatic component of surface pressure, $\Pi_{el} = \Pi - \Pi_0$, plotted vs. $A^{-3/2}$ for portions of the same experimental curves.

Another feature of the experimental Π(A) isotherms on the surface of the investigated KCl solutions is that they are very reproducible despite the partial aggregation of the particles. This is illustrated in Fig. 6a (0.1 mM KCl) and Fig. 6b (1 mM KCl), where we observe coincidence of the Π(A) isotherms obtained upon expansion of the particle monolayer in three consecutive cycles. Similar coincidence is observed also upon compression; see Fig. 6c and d, where the data are plotted as Π vs. $A^{-3/2}$ in accordance with Eq. (4). However, a considerable hysteresis is also observed: the values of Π upon compression are systematically greater than those upon expansion (Fig. 6c,d). Because of the reproducibility of the Π(A) isotherms in the presence of KCl, in Table 1 the average values of C and Π_0 for three cycles are given.

4. Theoretical section

4.1. Analytical expression for the surface pressure

In our previous study [23], a theoretical model was developed, which yields the following formula for calculating the electrostatic component of surface pressure, Π_{el}, for a monolayer of charged colloidal particles at the interface between water and a nonpolar fluid (air, oil):

$$\Pi_{el} = \frac{\sigma_{pn}^2 R}{\varepsilon_n} F(\xi), \quad \xi \equiv \frac{2R}{L} = \left(\frac{\alpha}{\alpha_h}\right)^{-1/2} \tag{5}$$

Here, ε_n is the dielectric constant of the nonpolar fluid; σ_{pn} is surface electric charge density at the boundary particle/nonpolar fluid; L is the particle center-to-center distance; $2R$ is the value of L at close contact between two particles; as before, α is the area per particle in the monolayer; α_h is the minimal possible value of α at close contact; ξ is a dimensionless parameter; $F(\xi) \equiv F(\xi, 20)$ is a universal dimensionless function, which is obtained analytically in the form of series expansion and tabulated – see Table S1 in the Supporting Information appended to Ref. [23]. The points in Fig. 7 represent values of $F(\xi)$ from this table, which are plotted vs. $\xi^3 = (\alpha/\alpha_h)^{-3/2}$. These points comply with a linear dependence of slope 1.972 and correlation coefficient better than 0.9999. Hence, for sufficiently small ξ, the function $F(\xi)$ can be estimated from the *asymptotic* formula (Fig. 7):
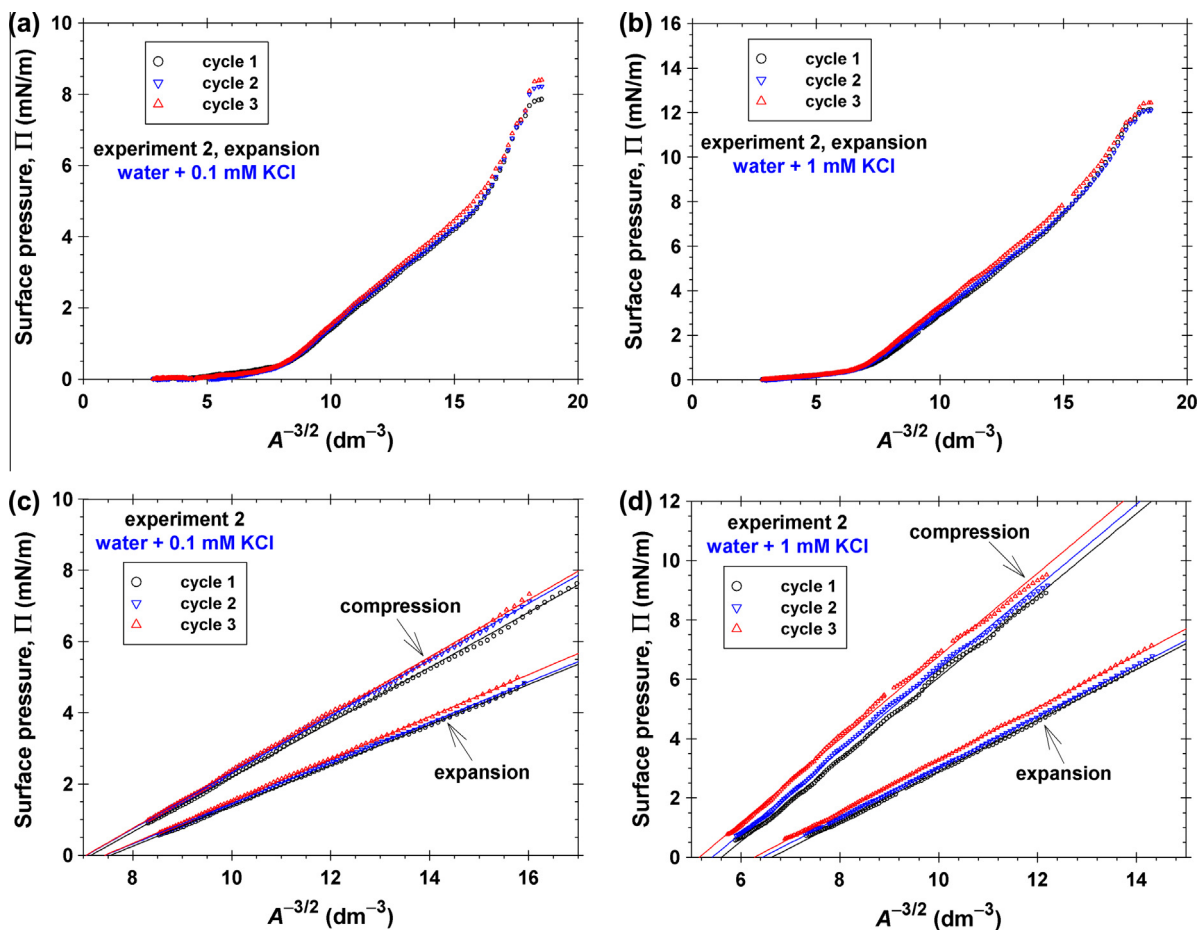
Fig. 6. Illustration of the reproducibility of surface-pressure isotherms in the presence of KCl in the aqueous phase: plots of the full Π vs. $A^{-3/2}$ curves for (a) 0.1 mM KCl and (b) 1 mM KCl for experiment #2, expansion. Plots of the linear parts of the Π vs. $A^{-3/2}$ curves for (c) 0.1 mM KCl and (d) 1 mM KCl for experiment #2, both compression and expansion.
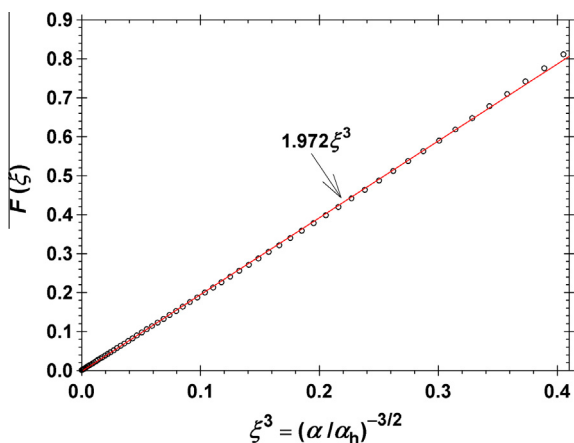

Fig. 7. Plot of the dimensionless function F vs. ξ^3, see Eq. (5); the points are exact numerical values from Ref. [23], whereas the solid line is fit by linear regression.

$$F \approx 1.972 \left(\frac{\alpha}{\alpha_h}\right)^{-3/2} \quad \text{for} \quad \left(\frac{\alpha}{\alpha_h}\right)^{-3/2} \leqslant 0.4 \qquad (6)$$

Note that the condition $(\alpha/\alpha_h)^{-3/2} \leqslant 0.4$ is satisfied for all data in Figs. 3d, 5b and 6c,d. The simple form of Eq. (6) makes easier the quantitative interpretation of surface pressure isotherms.

It should be mentioned that Eq. (5) presumes that the electrostatic repulsion between the particles in the monolayer is due to charges of surface density σ_{pn} located at the particle/nonpolar fluid interface (Fig. 1a). Eq. (5) is applicable also to the case when the electric field in the nonpolar fluid is created by charges of surface density σ_{pw} located at the particle/water interface (Fig. 1b). In the latter case, σ_{pn} in Eq. (5) should be formally expressed in terms of σ_{pw} using Eqs. (27) and (29) in Ref. [23].

In view of Eqs. (4)–(6), the total surface pressure can be expressed in the form:

$$\Pi = 1.972 \frac{\sigma_{pn}^2 R}{\varepsilon_n} \left(\frac{\alpha}{\alpha_h}\right)^{-3/2} + \Pi_0 \qquad (7)$$

Π_0 is an additive constant that is to be determined from the fit of experimental data.

In the model [23], square (rather than hexagonal) lattice of particles has been assumed for simplicity, and the particles have been modelled as squares of side $2R$. In such a case, the excluded area per particle and the particle charge can be expressed as follows:

$$\alpha_h = (2R)^2 \qquad (8)$$

$$Ze = (2R)^2 |\sigma_{pn}| \qquad (9)$$

where e is the elementary electric charge and Z is the average number of elementary charges per particle. Substituting α_h and σ_{pn} from Eqs. (8) and (9) into Eq. (7), we obtain:

$$\Pi = 0.986 \frac{(Ze)^2}{\varepsilon_n \alpha^{3/2}} + \Pi_0 \qquad (10)$$

Eq. (10) is in the basis of our subsequent analysis (see below). Note that in Eq. (10) α and Z are the physical mean area and charge per particle. It is remarkable the parameters of the auxiliary square-lattice model used in Ref. [23] to derive Eq. (5) (such as σ_{pn} and R) do not appear in Eq. (10). Indeed, the results of this derivation are not expected to be sensitive to the use of square or hexagonal lattice (with the same α and Z), because Π is a macroscopic quantity that is obtained by averaging over the interface; see Ref. [23] for details.

4.2. Effect of aggregation on the surface pressure of charged particles

Let us compare the surface pressures of a monolayer of charged particles, State 1 in Fig. 8a, with the surface pressure of the same monolayer in State 2 (Fig. 8b), in which the same particles have formed aggregates of aggregation number n. Then, the number of aggregates is $N_a = N/n$, where N is the total number of particles. If we consider the aggregates in the State 2 as bigger particles, their charge and area per particle are

$$Z = nZ_1, \quad \alpha = \frac{A}{N_a} = \frac{nA}{N} \qquad (11)$$

where Z_1 is the number of charges per one particle. Substituting Z and α from Eq. (11) in Eq. (10), we obtain:

$$\Pi = 0.986 \frac{(Z_1 e)^2 N^{3/2}}{\varepsilon_n} \frac{n^{1/2}}{A^{3/2}} + \Pi_0 \qquad (12)$$

Eq. (12) predicts that the electrostatic component of surface pressure, $\Pi_{el} = \Pi - \Pi_0$, should increase proportional to $n^{1/2}$, i.e. the surface pressure of a monolayer of charged particles should increase with the particle aggregation. This result can explain the rise of the slope of the experimental plots in Figs. 3d and 5b with the increase of n upon aggregation.

In view of Eqs. (10) and (11), the result $\Pi \propto n^{1/2}$ is due to the fact that the effect of aggregation on Π through the increase of Z prevails over the effect of the rise of α. These effects could be seen in the photographs, e.g. Fig. 3b, where the aggregates are surrounded by markedly larger empty areas than the single particles.

4.3. Data processing and numerical results

The value of the total number of particles between the barriers of the Langmuir trough, N, which enters Eq. (12), is known for Experiments 1 and 2 (see Table 2) from the experimental plots of α vs. A; see Fig. A2 in Appendix A. The greater N for the Experiment 2 indicates that in the respective batch the particles have had a lower charge, so we had to spread more droplets from the suspension in order to detect values of Π, which are comparable with those measured in the Experiment 1. The value of N is expected to be the same for all compression/expansion cycles within a given experiment, because no indications for particle detachment have been observed. Indeed, the aforementioned plots of α vs. A are always straight lines through the coordinate origin, viz. $A = N\alpha$.

From the slope C of the Π vs. $A^{-3/2}$ plots in Table 1, using Eq. (12) we calculated the product $Z_1 n^{1/4}$; see Table 3. Furthermore, to estimate separately the values of Z_1 and n, we have to make certain assumptions. Reasonable assumptions are: (i) $n = 1$ (no aggregation) for water, cycle 1, and (ii) $Z_1 = $ const. for all subsequent cycles, for which the value of n can be calculated knowing Z_1. Because $n = 1$ for water, cycle 1, the respective value of $Z_1 n^{1/4} = 1.58 \times 10^5$ is equal to the constant charge Z_1, which has been used to calculate n for the subsequent runs of Experiment 1. The obtained n values are also given in Table 3.

As seen in Table 3, in the case of Experiment 1, the aggregation number increases from $n = 1$ (cycle 1) to $n \approx 2.3$ (cycle 4), which is in qualitative agreement with the optical observations; see also Fig. 9a. Quantitative agreement between the values of n calculated from the $\Pi(A)$ isotherms and those determined by statistical
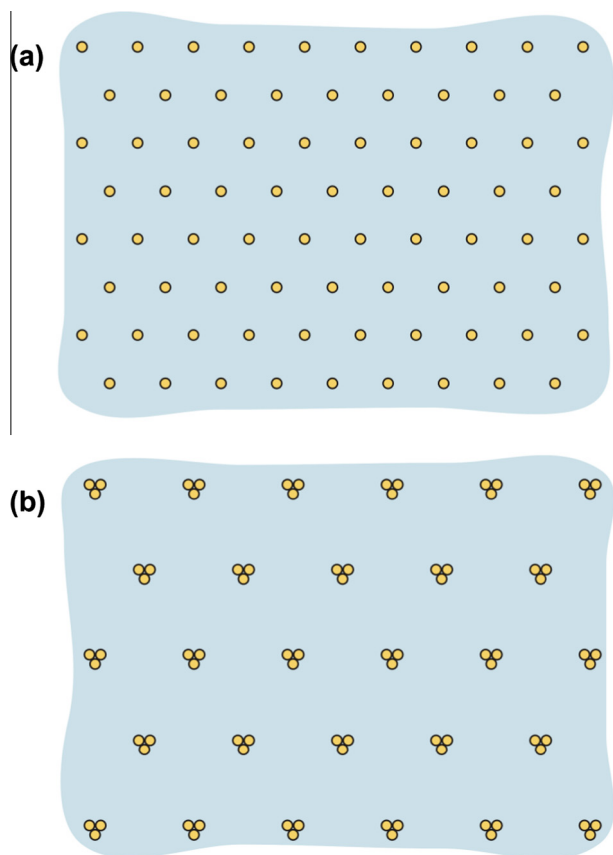
Fig. 8. Sketch of an ordered monolayer of charged particles at a liquid interface. (a) The monolayer consists of single particles. (b) An imaginary monolayer that consists of the same particles but in the form of aggregates from n particles ($n = 3$).

Table 2
Number of particles in the monolayer, N, surface charge density, σ, and area per surface charge, A_1, for Experiments 1 and 2.

Experiment	N	σ (μC/cm^2)	A_1 (nm^2)
#1, water	21.7×10^6	0.102	157
#2, water	28.6×10^6	0.071	227

Table 3
Values of $Z_1 n^{1/4}$ and n determined from the slope C in Table 1 using Eq. (12).

Run	$Z_1 n^{1/4}$	n
Experiment 1 (compression)		
Water, cycle 1	1.58×10^5	1
Water, cycle 2	1.72×10^5	1.39
Water, cycle 3	1.85×10^5	1.89
Water, cycle 4	1.94×10^5	2.29
Experiment 2 (compression)		
Water, cycle 1	1.09×10^5	1.00
Water, cycle 2	1.09×10^5	1.00
Water, cycle 3	1.12×10^5	1.11
0.1 mM KCl[a]	1.51×10^5	3.47[b]
1.0 mM KCl[a]	2.00×10^5	10.8[b]

[a] The parameter values for KCl solutions are average over three cycles.
[b] Lower limit of n estimated assuming that $Z_1 = 1.09 \times 10^5$, as for the water surface, cycle 1.
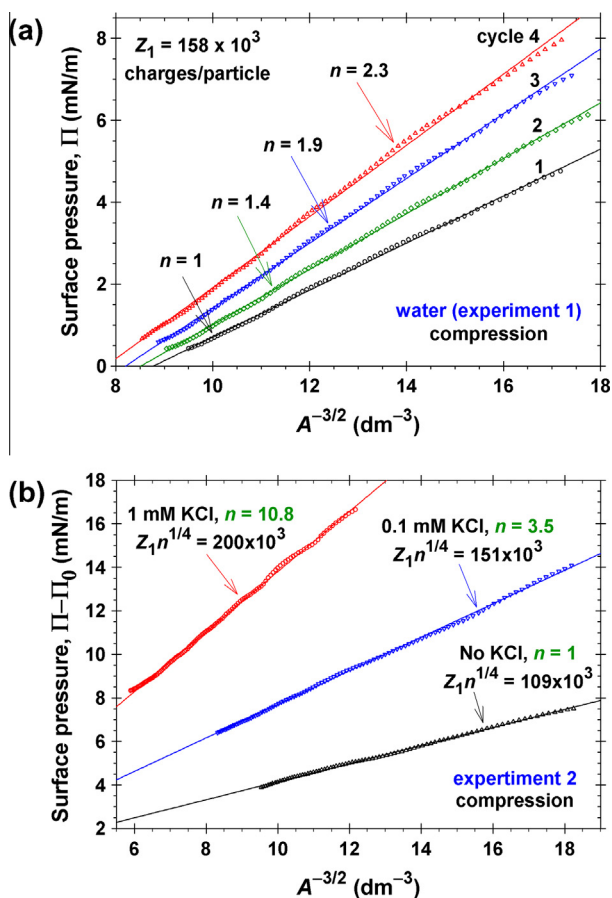
Fig. 9. Plots of Π vs. $A^{-3/2}$ together with the parameter values determined from the slopes of the lines using Eq. (12). (a) Lines from Fig. 3d together with the determined values of the mean aggregation number n. (b) Lines from Fig. 5b together with the determined values of $Z_1 n^{1/4}$; for the line without KCl, $n = 1$ is assumed and $Z_1 = 109 \times 10^3$ is determined; for the lines with 0.1 and 1 mM KCl, the lower limit of the n value is estimated assuming that Z_1 is the same as in the case without KCl.

analysis of photographs demands performing a new series of experiments, in which the area between the barriers, A, is varied in a step-wise manner and photos are taken at each step. Such series of experiments is labor consuming and could be a subject of a subsequent study.

In the case of Experiment 2, the particles have a lower charge, the repulsion between them is weaker and the aggregation is stronger in this system. In the case of monolayers spread on the surface of water (no salt), the optical observations of the monolayer indicate that the particles are predominantly in monomeric form, with few aggregates (Fig. 4a). We assumed that $n = 1$ for cycle 1 on the surface of water and determined Z_1 for this cycle. Further, assuming that Z_1 has the same value in all subsequent cycles, we found that $n = 1$ for cycle 2 and $n = 1.11$ for cycle 3; see Table 3.

In the presence of KCl in the water phase, a pronounced aggregation is observed; see Fig. 4b and c. As before, from the slopes of the plots of Π vs. $A^{-3/2}$ we can determine only the product $Z_1 n^{1/4}$, see Eq. (12), but we cannot separately determine Z_1 and n. However, we can estimate the lower limit of n assuming (approximately) that $Z_1 = 1.09 \times 10^5$, as for the surface of water (see Table 3). Thus, for the experiments with 0.1 and 1.0 mM KCl we obtain that the lower limits of aggregation number are, respectively, $n = 3.47$ and 10.8; see also Fig. 9b. The latter two values are certainly underestimated, because the use of the value of Z_1 for

pure water could be a rough approximation in the presence of KCl (see the discussion in Section 5.3). Indeed, it is more likely that the aggregation is due to a lower value of Z_1 in the presence of KCl, which would lead to a greater value of n, in order to have the same product $Z_1 n^{1/4}$ (see Table 3).

From the determined Z_1 for Experiments 1 and 2, water, cycle 1, we further estimated the surface electric charge density, σ, under the assumption that the charges that create the electric field are located on the particle/air interface. (Arguments in favor of this assumption are discussed in Section 5.3). The following formula was used:

$$2\pi R_p^2 (1 - \cos\theta)\sigma = Z_1 e \qquad (13)$$

In our case, the mean particle radius is $R_p = 1.92$ μm and the contact angle is $\theta = 94°$; in Eq. (13), we have used the approximation $\alpha_c \approx \theta$, which holds for relatively small particles like those used in our experiments. The values of σ determined from Eq. (13) and the values of the area per surface charge, A_1, are given in Table 2 for Experiments 1 and 2. For the Experiment 2, σ is with about 30% lower than for the Experiment 1. Both values of σ are slightly lower than those in our previous study [23]. For example, the lower σ for silica particles reported in Ref. [23] is 0.12 μC/cm², which is greater than the values of σ in Table 2.

5. Discussion

5.1. The driving force of particle aggregation

The results in the present article and their interpretation on the basis of Eq. (12) indicate that the aggregation of charged particles on the air/water interface leads to enhancement of their surface pressure Π. The first point that calls for discussion is the reason for surface aggregation of the used charged particles. An attractive force that can overcome the powerful electrostatic repulsion is needed. The gravity induced capillary attraction between floating particles [54,55] cannot be the reason for aggregation, because the weight of our particles is too small. Horozov and Binks [15] proposed that the reason for aggregation can be the attractive force between capillary quadrupoles, F_q, which is due to out-of-plane undulations of the contact lines on particle surfaces [56–61]. These undulations are related to the hysteresis of three-phase contact angle, which is present as a rule at solid surfaces (even at smooth ones), its absence being exclusion [62–66]. Because $F_q \propto L^{-5}$, it could overcome the electrostatic repulsion ($F_{ER} \propto L^{-4}$) at short distances. The distance, at which $F_{ER} + F_q = 0$, corresponds to the position of the energy barrier to particle aggregation. To check whether such distance really exists for our charged particles, in this equation we substitute the expressions for F_{ER} from Eq. (1) and F_q from Refs. [56,57]:

$$\frac{3(2DZ_1 e R_p \sin^3\theta)^2}{2\varepsilon_n L^4 (1 - \cos\theta)^2} - 48\pi\gamma H^2 \frac{r_c^4}{L^5} = 0, \qquad (14)$$

In the expression for F_{ER}, Eq. (1), we have substituted p_d from Eq. (2) and σ from Eq. (13). In the expression for F_q [the second term in Eq. (14)], γ is the surface tension of the liquid interface and H is the amplitude of contact-line undulations; the cosine in the formula for F_q has been set equal to 1, which corresponds to the energetically most favorable configuration of the two interacting capillary quadrupoles. Substituting typical parameter values, $\theta = 90°$; $R_p = r_c = 2$ μm, $L = 3R_p = 6$ μm; $\gamma = 72$ mN/m; $\varepsilon_n = 1$; $e = 4.80 \times 10^{-10}$ statcoulombs; $Z_1 = 10^{-5}$ (see Table 3), and $D(\theta, \varepsilon_{pn}) = 0.3135$ from Table 1 in Ref. [33] for $\varepsilon_{pn} = 4$, from Eq. (14) we calculate $H = 0.433$ μm, which is a reasonable value for the amplitude of contact line undulations on the surface of a particle of diameter ≈ 4 μm. Hence, the reason for aggregation of

the charged particles can be really the attraction between capillary quadrupoles. At close contact, short range attractive forces, such as the van der Waals and hydrophobic surface forces [67], can further enhance the interparticle attraction.

5.2. Limited aggregation of charged particles at a liquid interface

A second point that deserves discussion is the presence of long linear portions in the Π vs. $A^{-3/2}$ (see e.g. Fig. 9), which in view of Eq. (12) indicate that the average aggregation number, n, has been constant during the respective compression or expansion of the particle monolayer. This finding leads to the concept of *limited aggregation* of particles, which is logically analogous to the limited coalescence in Pickering emulsions [68–70]. Indeed, the particle aggregation enhances the electrostatic repulsion between the aggregates and this leads to a rise of the electrostatic barrier to aggregation and eventually – to ceasing of aggregation. In other words, we are dealing with a negative feedback. Moreover, the particle aggregates should behave as capillary multipoles of higher order [58,60] that experience capillary attraction of shorter range and smaller amplitude, which should additionally increase the height of the barrier to coalescence upon aggregation.

In the case of particles of lower charge, the barrier to aggregation is lower and the limited coalescence is expected to occur faster. This seems to be the case with Experiment 2, where the isotherms obtained upon compression (or upon expansion) are very reproducible (see eg. Fig. 6) that indicates completed limited coalescence. The hysteresis, i.e. the difference between compression and expansion (Fig. 6c,d), could be explained with the presence of loosely connected aggregates that coalesce upon compression, but split upon expansion.

The rise of Π with the number of compression/expansion cycle in the case of Experiment 1 (Fig. 3c) could be explained in the following way. In this experiment, the particle charge is greater (see Table 2), and the barrier to aggregation is higher. Then, it is possible that the particles can overcome the barrier only in the most compressed state of the monolayer, i.e. during the interval of 100 s after the end of compression and before the start of the subsequent expansion. In such case, the process of limited aggregation would happen in a stepwise manner, as experimentally observed; see Fig. 9a.

5.3. Origin of the surface charges and effect of electrolyte

The third point that calls for discussion is the origin of surface charges of the hydrophobized silica particles and the effect of electrolyte on surface pressure. First, let us check whether it is possible the detected electrostatic effects to be due to electric charges at the particle/water interface. For $\kappa R_p \gg 1$ (thin electric double layer), we can use the Gouy equation that connects the surface charge density and the surface potential for a planar interface:

$$\frac{\sigma_{pw}}{e} = \frac{4I}{\kappa}\sinh\left(\frac{\Phi_s}{2}\right), \quad \Phi_s \equiv \frac{e|\varphi_s|}{kT} \tag{15}$$

where I is the ionic strength of the aqueous solution; k is the Boltzmann's constant; T is the absolute temperature; φ_s and Φ_s are the dimensional and dimensionless electric potentials of the particle/water interface. Furthermore, eliminating p_d between Eqs. (2) and (3), and substituting σ_{pw} from Eq. (15), we derive:

$$\sigma = \frac{\varepsilon_n(1+\cos\theta)e}{2\pi\varepsilon_w L_B R_p D \sin^3\theta}\sinh\left(\frac{\Phi_s}{2}\right) \tag{16}$$

Here, we have used the formula $\kappa^2 = 8\pi L_B I$, where $L_B = e^2/(\varepsilon_w kT)$ is the Bjerrum length; $L_B = 0.72$ nm for water at 25 °C; as before, we have used the approximation $\alpha_c = \theta$ for small particles. Note that

the coefficient before the hyperbolic sine in Eq. (16) does not contain the solution's ionic strength, I. In view of Eqs. (1)–(3), the physical meaning of Eq. (16) is as follows: The existence of surface potential Φ_s at the particle/water interface creates the same electrostatic interparticle repulsion as surface charge density σ [given by Eq. (16)] at the particle/air interface. Substituting typical parameter values, $\theta = 90°$; $R_p = 2$ μm, $\varepsilon_n = 1$; $\varepsilon_w = 78.2$, $D = 0.3135$ (see above) and $\Phi_s = 2.53$ corresponding to $\varphi_s = -65$ mV (see Fig. 2), we calculate that the latter value of Φ_s at the particle/water interface is equivalent to surface charge density $\sigma = 0.118 \times 10^{-3}$ μC/cm^2 at the particle/air interface. The latter value is about thousand times smaller than the value of σ obtained from the slopes of our experimental $\Pi(A)$ isotherms; see Table 2. In view of the hyperbolic sine in Eq. (16), to get σ of the order of 0.1 μC/cm^2 (as in Table 2) we should have $|\varphi_s| \approx 415$ mV, which is unrealistic in view of the zeta potential data in Fig. 2. Hence, we can conclude that charges at the particle/water interface cannot be the reason for the observed electrostatic repulsion between the particles in the monolayer. In other words, the electrostatic surface pressure measured in our experiments is due to charges at the particle/air interface.

In general, Eq. (16) can serve as a quantitative criterion for establishing whether the electrostatic repulsion between particles at liquid interfaces is due to charges at the particle/water or particle/air interface. Because of the presence of R_p in the denominator of Eq. (16), the contribution of the particle/water interface is expected to be greater for smaller particles.

The origin of the surface charge on the particle/air (or particle/oil) interface already has been a subject of discussions in the literature [15,38]. As mentioned in Section 2, the possible reason for these surface charges could be adsorption of ions from the air on the particles during their contact with the atmosphere. The silica particles have a higher dielectric constant ($\varepsilon_p = 3.9$) than the nonpolar fluid (air, $\varepsilon_n = 1$), and for this reason they attract the charges dispersed in atmospheric air because of the electrostatic image force; see e.g. Ref. [71]. These charges are H$^+$ and OH$^-$, which are due to dissociated water molecules [39–41]. Depending on whether the solid is acidic or basic, the preferential adsorption of OH$^-$ or H$^+$ ions on the solid/air interface leads to negative or positive surface potentials, respectively. Thus, for silica surface a potential $\Delta V = -172 \pm 15$ mV was detected by Kelvin force microscopy for relative humidity of air from 30% to 70% [41]. In contact with the water vapors in air, water is chemisorbed at the silica surface, forming a silanol (Si–OH) layer covered with an adsorption bilayer of H-bonded water molecules [72,73]. In this layer, OH$^-$ ions could also bind, because they form stronger H-bonds than the H$_2$O molecules.

Our experiments indicate that the hydrophobization by DCDMS does not remove the ability of the silica surface to adsorb OH$^-$ ions from the air. The hydrophobization by DCDMS consists in replacement of Si–OH groups by (SiO)$_2$–Si–(CH$_3$)$_2$ groups [74,75]. Moreover, it has been found that not all surface silanol groups interact with the hydrophobizing agent; e.g., only a small fraction of the mutually H-bonded OH groups react with the silanizing agent [76]. In our case, the value of contact angle $\theta = 94°$ indicates a relatively low degree of hydrophobization. Hence, we could hypothesize that a large fraction of the hydrophobized particle/air interface is covered by silanol groups with an adjacent adsorption bilayer of water molecules and OH$^-$ ions, whereas the silanized groups form separate hydrophobic "islands". It should be also noted that the binding of OH$^-$ to the particle surface is strong enough to preserve the negative surface charge upon particle storage in IPA, as experimentally observed.

Finally, a possible reason for the enhancement of aggregation with the rise of KCl concentration can be the migration of K$^+$ ions from the aqueous phase to the particle/air interface, that leads to

a decrease of the net particle charge Z. Indeed, the subsurface layer of the particle/water interface is enriched in K$^+$ counterions (see Fig. 1b), from where they could move toward the particle/air interface attracted by its negative charge. The medium that favors such migration could be the fraction of the particle/air interface, which is covered by silanol groups with an adjacent adsorption bilayer of water molecules and OH$^-$ ions (see above). Similar migration of OH$^-$ ions along the silica/air interface under the action of tangential electric potential difference has been already observed [39].

It should be also noted that in the presence of 50 mM KCl in the aqueous phase, we observed the formation of large two-dimensional domains of aggregated particles at the air/water interface. This is probably due to a complete suppression of the negative charge of the particle/air interface because of the transfer of potassium cations. In the experiments by Horozov et al. [13], the electrolyte concentration was raised up to 1 M NaCl without suppressing the electrostatic interparticle forces. However, in these experiments the nonpolar fluid was octane (rather than humid air), which most probably blocks the migration of the hydrophilic Na$^+$ ions to the particle/oil interface.

6. Conclusions

In the present study, we investigate the effect of aggregation on the surface pressure, Π, of monolayers from charged μm-sized colloidal particles on the air/water interface. In such monolayers, Π is completely due to the soft and long-range electrostatic repulsion between the particles mediated by their electrostatic field in the nonpolar fluid (in the air), where Debye screening is absent [3]. The aggregation of the charged particles is engendered by the attraction between capillary quadrupoles (due to undulated contact lines on the particle surfaces) [56–60], which turns out to be strong enough to overcome the powerful electrostatic repulsion between the particles at sufficiently short distances between them [15]; see Eq. (14). The aggregation gives rise to two effects, which are acting in the opposite directions. (i) Aggregates have higher charge and repel each other stronger than single particles. (ii) The distances between the aggregates are larger than between the single particles (in the beginning of aggregation), which leads to decrease of the electrostatic repulsion. Our theoretical model leads to the conclusion that the first effect always prevails and that Π should linearly increase with $n^{1/2}$ (with the square root of aggregation number); see Eq. (12). This conclusion is in agreement with the obtained experimental Π(A) isotherms, which indicate an increase of surface pressure with the rise of aggregation in the particle monolayer. From the experimental Π(A) curves, one can determine the mean aggregation number, n; see Table 3. There are indications that the stronger electrostatic repulsion between the bigger aggregates leads to *limited aggregation* in monolayers of charged particles: the rise of the electrostatic barrier in the course of aggregation prevents the further coalescence of aggregates that have reached a sufficiently large size.

The presence of salt in the aqueous phase also produces two effects acting in the opposite directions. (i) The salt promotes the aggregation (n increases), which tends to increase Π. However, (ii) the salt reduces the surface charge Z (see Section 5.3) and thus tends to lower Π. Depending on the specific system, the first or the second tendency could prevail. In our case – this is the rise of n. In other words, the salt reduces the surface charge, Z, and enhances the aggregation, which in a final reckoning leads to a rise of Π. As a result, we observe an apparently paradoxical effect – the addition of salt in the aqueous phase enhances the electrostatic surface pressure.

The results in the present article contribute for a better understanding of the factors that control the interactions in monolayers of charged particles at liquid interfaces, which have found various applications, e.g., for micropatterning of surfaces and for control of their reflectance [5–8]. The results could be also important for the quantitative description of interactions between charged macromolecules, e.g. globular proteins, in adsorption layers.

Appendix A. Supplementary material

Supplementary data associated with this article can be found, in the online version, at http://dx.doi.org/10.1016/j.jcis.2015.09.075.

References

[1] H. Schuller, Modellversuche zur Spreitung von Kolloid-Partikeln, Kolloid Z. Z. Polym. 216 (1967) 380–383.
[2] E. Sheppard, N. Tcheurekdjian, Monolayer studies. IV. Surface films of emulsion latex particles, J. Colloid Interface Sci. 28 (1968) 481–486.
[3] R. Aveyard, J.H. Clint, D. Nees, V.N. Paunov, Compression and structure of monolayers of charged latex particles at air/water and octane/water interfaces, Langmuir 16 (2000) 1969–1979.
[4] Y. Zhao, J. Wang, G. Mao, Colloidal subwavelength nanostructures for antireflection optical coatings, Opt. Lett. 30 (2005) 1885–1887.
[5] M.A. Ray, L. Jia, Micropatterning by non-densely packed interfacial colloidal crystals, Adv. Mater. 19 (2007) 2020–2022.
[6] W.-L. Min, P. Jiang, B. Jiang, Large-scale assembly of colloidal nanoparticles and fabrication of periodic subwavelength structures, Nanotechnology 19 (2008) 475604.
[7] M.A. Ray, N. Shewmon, S. Bhawalkar, L. Jia, Y. Yang, E.S. Daniels, Submicrometer surface patterning using interfacial colloidal particle self-assembly, Langmuir 25 (2009) 7265–7270.
[8] S.P. Bhawalkar, J. Qian, M.C. Heiber, L. Jia, Development of a colloidal lithography method for patterning nonplanar surfaces, Langmuir 26 (2010) 16662–16666.
[9] O.J. Cayre, V.N. Paunov, Fabrication of microlens arrays by gel trapping of self-assembled particle monolayers at the decane–water interface, J. Mater. Chem. 14 (2004) 3300–3302.
[10] Y. Sun, S.R. Forrest, Organic light emitting devices with enhanced outcoupling via microlenses fabricated by imprint lithography, J. Appl. Phys. 100 (2006) 073106.
[11] C.J. Bettinger, R. Langer, J.T. Borenstein, Engineering substrate micro- and nanotopography to control cell function, Angew. Chem., Int. Ed. 48 (2009) 5406–5415.
[12] L. Isa, K. Kumar, M. Müller, J. Grolig, M. Textor, E. Reimhult, Particle lithography from colloidal self-assembly at liquid–liquid interfaces, ACS Nano 4 (2010) 5665–5670.
[13] T.S. Horozov, R. Aveyard, J.H. Clint, B.P. Binks, Order-disorder transition in monolayers of modified monodisperse silica particles at the octane–water interface, Langmuir 19 (2003) 2822–2829.
[14] E.J. Stancik, M. Kouhkan, G.G. Fuller, Coalescence of particle-laden fluid interfaces, Langmuir 20 (2004) 90–94.
[15] T.S. Horozov, B.P. Binks, Particle behavior at horizontal and vertical fluid interfaces, Colloids Surf., A 267 (2005) 64–73.
[16] T.S. Horozov, R. Aveyard, J.H. Clint, B. Neumann, Particle zips: vertical emulsion films with particle monolayers at their surfaces, Langmuir 21 (2005) 2330–2341.
[17] H. Xu, J. Kirkwood, M. Lask, G. Fuller, Charge interaction between particle-laden fluid interfaces, Langmuir 26 (2010) 3160–3164.
[18] V. Garbin, J.C. Crocker, K.J. Stebe, Forced desorption of nanoparticles from an oil–water interface, Langmuir 28 (2012) 1663–1667.
[19] S. Crossley, J. Faria, M. Shen, D.E. Resasco, Solid nanoparticles that catalyze biofuel upgrade reactions at the water/oil interface, Science 327 (2010) 68–72.
[20] V. Garbin, J.C. Crocker, K.J. Stebe, Nanoparticles at fluid interfaces: exploiting capping ligands to control adsorption, stability and dynamics, J. Colloid Interface Sci. 387 (2012) 1–11.
[21] S. Reynaert, P. Moldenaers, J. Vermant, Control over colloidal aggregation in monolayers of latex particles at the oil–water interface, Langmuir 22 (2006) 4936–4945.
[22] C. Monteux, E. Jung, G.G. Fuller, Mechanical properties and structure of particle coated interfaces: influence of particle size and bidisperse 2D suspensions, Langmuir 23 (2007) 3975–3980.
[23] P.V. Petkov, K.D. Danov, P.A. Kralchevsky, Surface pressure isotherm for a monolayer of charged colloidal particles at a water/nonpolar-fluid interface: experiment and theoretical model, Langmuir 30 (2014) 2768–2778.

[24] P. Pieranski, Two-dimensional interfacial colloidal crystals, Phys. Rev. Lett. 45 (1980) 569–572.

[25] A.J. Hurd, The electrostatic interaction between interfacial colloidal particles, J. Phys. A: Math. Gen. 18 (1985) L1055–L1060.

[26] V.N. Paunov, Electrostatic interaction between charged colloid particles entrapped in a thin electrolyte film: confinement effects, Colloid Polym. Sci. 281 (2003) 701–707.

[27] A. Würger, L. Foret, Capillary attraction of colloidal particles at an aqueous interface, J. Phys. Chem. B 109 (2005) 16435–16438.

[28] M. Oettel, S. Dietrich, Colloidal interactions at fluid interfaces, Langmuir 24 (2008) 1425–1441.

[29] B.J. Park, J.P. Pantina, E.M. Furst, M. Oettel, S. Reynaert, J. Vermant, Direct measurements of the effects of salt and surfactant on interaction forces between colloidal particles at water–oil interfaces, Langmuir 24 (2008) 1686–1694.

[30] R. Aveyard, B.P. Binks, J.H. Clint, P.D.I. Fletcher, T.S. Horozov, B. Neumann, V.N. Paunov, J. Annesley, S.W. Botchway, D. Nees, A.W. Parker, A.D. Ward, A.N. Burgess, Measurement of long-range repulsive forces between charged particles at an oil–water interface, Phys. Rev. Lett. 88 (2002) 246102.

[31] T.S. Horozov, R. Aveyard, B.P. Binks, J.H. Clint, Structure and stability of silica particle monolayers at horizontal and vertical octane–water interfaces, Langmuir 21 (2005) 7405–7412.

[32] K.D. Danov, P.A. Kralchevsky, M.P. Boneva, Electrodipping force acting on solid particles at a fluid interface, Langmuir 20 (2004) 6139–6151.

[33] K.D. Danov, P.A. Kralchevsky, Electric forces induced by a charged colloid particle attached to the water–nonpolar fluid interface, J. Colloid Interface Sci. 298 (2006) 213–231.

[34] K.D. Danov, P.A. Kralchevsky, M.P. Boneva, Shape of the capillary meniscus around an electrically charged particle at a fluid interface. comparison of theory and experiment, Langmuir 22 (2006) 2653–2667.

[35] M.E. Leunissen, A. van Blaaderen, A.D. Hollingsworth, M.T. Sullivan, P.M. Chaikin, Electrostatics at the oil–water interface, stability, and order in emulsions and colloids, Proc. Natl. Acad. Sci. 104 (2007) 2585–2590.

[36] M.E. Leunissen, J. Zwanikken, R. van Roij, P.M. Chaikin, A. van Blaaderen, Ion partitioning at the oil–water interface as a source of tunable electrostatic effects in emulsions with colloids, Phys. Chem. Chem. Phys. 9 (2007) 6405–6414.

[37] M.P. Boneva, N.C. Christov, K.D. Danov, P.A. Kralchevsky, Effect of electric-field-induced capillary attraction on the motion of particles at an oil–water interface, Phys. Chem. Chem. Phys. 9 (2007) 6371–6384.

[38] M.P. Boneva, K.D. Danov, N.C. Christov, P.A. Kralchevsky, Attraction between particles at a liquid interface due to the interplay of gravity-and electric-field-induced interfacial deformations, Langmuir 25 (2009) 9129–9139.

[39] R.F. Gouveia, C.A.R. Costa, F. Galembeck, Water vapor adsorption effect on silica surface electrostatic patterning, J. Phys. Chem. C 112 (2008) 17193–17199.

[40] R.F. Gouveia, F. Galembeck, Electrostatic charging of hydrophilic particles due to water adsorption, J. Am. Chem. Soc. 131 (2009) 11381–11386.

[41] R.F. Gouveia, J.S. Bernardes, T.R.D. Ducati, F. Galembeck, Acid–base site detection and mapping on solid surfaces by Kelvin force microscopy (KFM), Anal. Chem. 84 (2012) 10191–10198.

[42] C.L. Wirth, E.M. Furst, J. Vermant, Weak electrolyte dependence in the repulsion of colloids at an oil–water interface, Langmuir 30 (2014) 2670–2675.

[43] K. Geisel, L. Isa, W. Richtering, The compressibility of pH-sensitive microgels at the oil–water interface: higher charge leads to less repulsion, Angew. Chem. 126 (2014) 5005–5009.

[44] K.D. Danov, P.A. Kralchevsky, Forces acting on dielectric colloidal spheres at a water/nonpolar-fluid Interface in an external electric field. 1. Uncharged particles, J. Colloid Interface Sci. 405 (2013) 278–290.

[45] K.D. Danov, P.A. Kralchevsky, Forces acting on dielectric colloidal spheres at a water/nonpolar-fluid Interface in an external electric field. 2. Charged particles, J. Colloid Interface Sci. 405 (2013) 269–277.

[46] G. Bakker, Kapillarität und Oberflächenspannung, in: Handbuch der Experimentalphysik, Band 6, Akademische Verlagsgesellschaft, Leipzig, 1928.

[47] K.G. Marinova, D. Christova, S. Tcholakova, E. Efremov, N.D. Denkov, Hydrophobization of glass surface by adsorption of poly(dimethylsiloxane), Langmuir 21 (2005) 11729–11737.

[48] P.M. Kolarž, D.M. Filipović, B.P. Marinković, Daily variations of indoor air-ion and radon concentrations, Appl. Radiat. Isot. 67 (2009) 2062–2067.

[49] M.A. Cohen Stuart, J.W. Mulder, Adsorbed polymers in aqueous media the relation between zeta potential, layer thickness and ionic strength, Colloids Surf. 15 (1985) 49–55.

[50] M. Lund, L. Vrbka, P. Jungwirth, Specific ion binding to nonpolar surface patches of proteins, J. Am. Chem. Soc. 130 (2008) 11582–11583.

[51] M. Lund, J. Heyda, P. Jungwirth, Ion binding to bio-molecules, in: W. Kunz (Ed.), Specific Ion Effects, World Scientific Publishing Co., London, 2010, pp. 217–230.

[52] M. Lund, R. Vácha, P. Jungwirth, Specific ion binding to macromolecules: effects of hydrophobicity and ion pairing, Langmuir 24 (2008) 3387–3391.

[53] P.A. Kralchevsky, K.D. Danov, G. Broze, A. Mehreteab, Thermodynamics of ionic surfactant adsorption with account for the counterion binding: effect of salts of various valency, Langmuir 15 (1999) 2351–2365.

[54] D.Y.C. Chan, J.D. Henry, R.L. White, The interaction of colloidal particles collected at fluid interfaces, J. Colloid Interface Sci. 79 (1981) 410–418.

[55] V.N. Paunov, P.A. Kralchevsky, N.D. Denkov, K. Nagayama, Lateral capillary forces between floating submillimeter particles, J. Colloid Interface Sci. 157 (1993) 100–112.

[56] D. Stamou, C. Duschl, D. Johannsmann, Long-range attraction between colloidal spheres at the air–water interface: the consequence of an irregular meniscus, Phys. Rev. E 62 (2000) 5263–5272.

[57] P.A. Kralchevsky, N.D. Denkov, K.D. Danov, Particles with an undulated contact line at a fluid interface: interaction between capillary quadrupoles and rheology of particulate monolayers, Langmuir 17 (2001) 7694–7705.

[58] K.D. Danov, P.A. Kralchevsky, B.N. Naydenov, G. Brenn, Interactions between particles with an undulated contact line at a fluid interface: capillary multipoles of arbitrary order, J. Colloid Interface Sci. 287 (2005) 121–134.

[59] J.C. Loudet, A.G. Yodh, B. Pouligny, Wetting and contact lines of micrometer-sized ellipsoids, Phys. Rev. Lett. 97 (2006) 018304.

[60] K.D. Danov, P.A. Kralchevsky, Capillary forces between particles at a liquid interface: general theoretical approach and interactions between capillary multipoles, Adv. Colloid Interface Sci. 154 (2010) 91–103.

[61] L. Botto, E.P. Lewandowski, M. Cavallaro Jr., K.J. Stebe, Capillary interactions between anisotropic particles, Soft Matter 8 (2012) 9957–9971.

[62] F.E. Bartell, J.W. Shepard, Surface roughness as related to hysteresis of contact angles. I. The system paraffin–water–air, J. Phys. Chem. 57 (1953) 211–215.

[63] V.M. Starov, Equilibrium and hysteresis contact angles, Adv. Colloid Interface Sci. 39 (1992) 147–173.

[64] A. Marmur, Thermodynamic aspects of contact angle hysteresis, Adv. Colloid Interface Sci. 50 (1994) 121–141.

[65] J. Drelich, J.D. Miller, R.J. Good, The effect of drop (bubble) size on advancing and receding contact angles for heterogeneous and rough solid surfaces as observed with sessile-drop and captive-bubble techniques, J. Colloid Interface Sci. 179 (1996) 37–50.

[66] S.D. Iliev, Static drops on an inclined plane: equilibrium modeling and numerical analysis, J. Colloid Interface Sci. 194 (1997) 287–300.

[67] J.N. Israelachvili, Intermolecular and Surface Forces, third ed., Academic Press, London, 2011.

[68] T.H. Whitesides, D.S. Ross, Experimental and theoretical analysis of the limited coalescence process: stepwise limited coalescence, J. Colloid Interface Sci. 169 (1995) 48–59.

[69] S. Arditty, C.P. Whitby, B.P. Binks, V. Schmitt, F. Leal-Calderon, Some general features of limited coalescence in solid-stabilized emulsions, Eur. Phys. J. E 11 (2003) 273–281.

[70] K. Golemanov, S. Tcholakova, P.A. Kralchevsky, K.P. Ananthapadmanabhan, A. Lips, Latex-particle-stabilized emulsions of anti-Bancroft type, Langmuir 22 (2006) 4968–4977.

[71] L.D. Landau, E.M. Lifshitz, Electrodynamics of Continuous Medium, Pergamon Press, Oxford, U.K., 1960.

[72] M.L. Hair, W. Hertl, Adsorption on hydroxylated silica surfaces, J. Phys. Chem. 73 (1969) 4269–4276.

[73] L.T. Zhuravlev, The surface chemistry of amorphous silica. Zhuravlev model, Colloids Surf. A 173 (2000) 1–38.

[74] J.A. Voorthuyzen, K. Keskin, P. Bergveld, Investigations of the surface conductivity of silicon dioxide and methods to reduce it, Surface Sci. 187 (1987) 201–211.

[75] M.L. Hair, W. Hertl, Reactions of chlorosilanes with silica surfaces, J. Phys. Chem. 73 (1969) 2372–2378.

[76] M.L. Hair, W. Hertl, Reaction of hexamethyldisilazane with silica, J. Phys. Chem. 75 (1971) 2181–2185.